Characterization of two distinct amorphous forms of valsartan by solid-state NMR

Marcin Skotnicki,[1,2] David C. Apperley,[2] Juan A. Aguilar,[2] Bartłomiej Milanowski,[1] Marek Pyda[3] and Paul Hodgkinson[2*]

[1]Department of Pharmaceutical Technology, Poznań University of Medical Sciences, ul. Grunwaldzka 6, 60-780 Poznań, Poland

[2]Department of Chemistry, Durham University, South Road, Durham, DH1 3LE, United Kingdom

[3]Department of Chemistry, Rzeszów University of Technology, 35-959 Rzeszów, Poland

[*]Corresponding author:

Paul Hodgkinson, Department of Chemistry, Durham University, South Road, Durham, DH1 3LE, UK.

Tel: +44 191 334 2019, E-mail: paul.hodgkinson@durham.ac.uk

ABSTRACT

Valsartan (VAL) is an antihypertensive drug marketed in an amorphous form. Amorphous materials can have different physicochemical properties depending on preparation method, thermal history etc., but the nature of such materials is difficult to study by diffraction techniques. This study characterizes two different amorphous forms of valsartan (AR and AM) using solid-state NMR (SSNMR) as a primary investigation tool, supported by solution-state NMR, FT-IR, TMDSC and dissolution tests. The two forms are found to be clearly distinct, with a significantly higher level of structural arrangement in the AR form, as observed in ^{13}C, ^{15}N and ^{1}H SSNMR. ^{13}C and ^{15}N NMR indicates that the fully amorphous material (AM) contains an approximately equal ratio of *cis–trans* conformers about the amide bond, whereas AR form exists mainly as one conformer, with minor conformational "defects". ^{1}H ultra-fast MAS NMR shows significant differences in the hydrogen bonding involving the tetrazole and acid hydrogens between the two materials, while ^{15}N NMR shows that both forms exist as an 1,2,3,4-tetrazole tautomer. NMR relaxation times show subtle differences in local and bulk molecular mobility, which can be connected with the glass transition, the stability of the glassy material and its response to ageing. Counter-intuitively the fully amorphous material is found to have a significantly lower dissolution rate than the apparently more ordered AR material.

ABSTRACT GRAPHICS

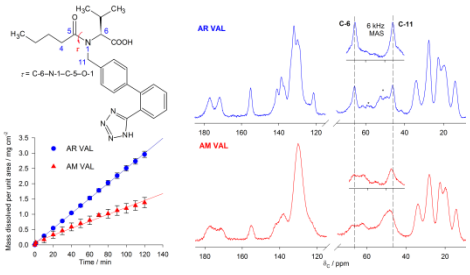

KEY WORDS

valsartan, amorphous form, *cis–trans* amide conformers, solid-state NMR, molecular mobility, glass transition, dissolution

INTRODUCTION

Valsartan (VAL, Figure 1A) is an antihypertensive drug belonging to the angiotensin II receptor antagonists class called sartans,[1] which is marketed in an amorphous form. Such solids differ from crystalline materials in lacking long-range order, although some short-range order may be present.[2, 3] Amorphous active pharmaceutical ingredients (APIs) have been used in the development of pharmaceutical solid formulations due to factors such as increased solubility and dissolution rate compared to crystalline forms.[4-6] However, amorphous APIs are usually less stable than their crystalline counterparts. The occurrence of polymorphism in crystalline pharmaceuticals and its impact on physicochemical properties is well documented,[7-10] but it is also known that amorphous materials can have different physicochemical properties, depending on previous thermal history, time of storage and preparation method.[11-15] Amorphous materials can exist in different kinetic states, and the term pseudopolyamorphism or relaxation polyamorphism has been used to describe this phenomenon.[2] Polyamorphism, the possible existence of two or more distinct amorphous forms of the same compound separated by a clear phase transition has been reported for inorganic compounds[16-18] and discussed in the context of pharmaceuticals,[2, 10, 12, 19] although, to our knowledge, there is no definitive example of polyamorphism in pharmaceutics.

A

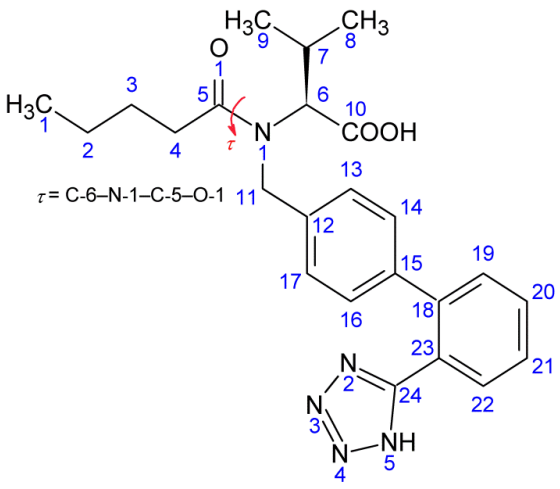

B

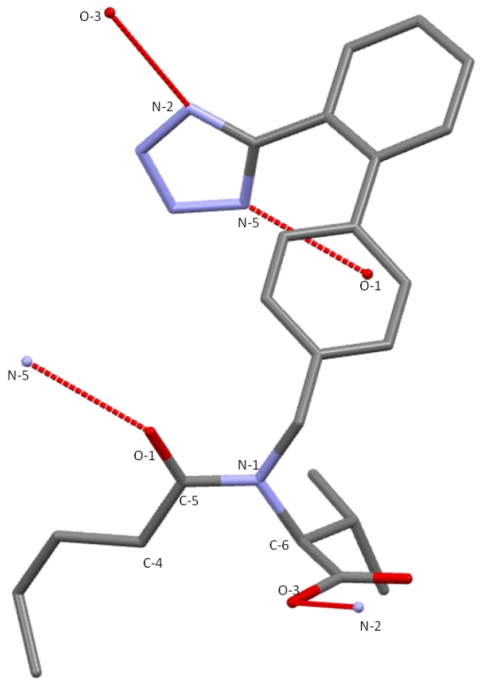

Figure 1. (A) Chemical structure of valsartan (*N*-[*p*-(*o*-1*H*-tetrazol-5-ylphenyl)benzyl]-*N*-valeryl-L-valine) with all carbons and nitrogens numbered. Numbering scheme used as in Refs.[20, 21] The dihedral angle C-6–N-1–C-5–O-1, *τ*, that determines the amide *cis* (*τ* ≈180°) vs *trans* (*τ* ≈ 0°) conformation, as defined in Ref.[21], is shown. (B) The structure of the independent molecule of valsartan in the asymmetric unit and hydrogen bonding adapted from Ref.[20] The *τ* torsion angle is ~171°, corresponding to the *cis* isomer. Hydrogens are omitted for clarity.

Despite a wide variety of analytical techniques available, the structural characterization of subtle differences between different amorphous forms of active pharmaceutical ingredients remains challenging. It is also important to understand the nature of molecular mobility in amorphous APIs, because molecular relaxation may take place during storage. Solid-state NMR (SSNMR) has been widely used to study molecular dynamics in pharmaceutics.[22-25] For example, Luthra *et al.* studied changes in molecular dynamics of model drug systems during annealing by Differential Scanning Calorimetry (DSC)[26] and ^{13}C NMR relaxation times.[27] They observed that in most cases annealing leads to longer T_1 and $T_{1\rho}$ NMR relaxation times, indicating a slowing of the local dynamics. Abdul-Fattah *et al.* observed that higher temperature annealing decreased molecular mobility as measured by isothermal calorimetry and improved chemical stability.[28]

Various analytical methods have been used to characterize the solid state of valsartan. Tran *et al*. studied the influence of various types of solvents on the re-crystallisation behaviour of two sources of valsartan by DSC, powder X-ray diffractrometry (PXRD) and scanning electron microscopy,[29] and found significant differences in morphology, structure and dissolution rate among the recrystallized samples. The lack of strong Bragg diffraction peaks in the PXRD results suggest, however, that most of the forms produced were essentially amorphous with different levels of local order rather than crystalline. The commercially available form (termed here the as-received, or AR, form) and the amorphous form obtained by quench-cooling (here called the AM form) were characterized by us using thermal methods and PXRD.[30] The studies revealed significantly different glass transition temperatures for both materials and a higher degree of structural ordering in the marketed form. The crystal structure of a highly crystalline form of valsartan and its ethanol solvate have been recently published,[20] characterized by various solid-state techniques and compared to the marketed amorphous form.

Solid-state NMR is a powerful technique for the characterization of solid pharmaceuticals.[22, 31, 32] SSNMR has the advantage of providing localised chemical information on the crystalline or amorphous state, unlike bulk methods such as DSC or PXRD. SSNMR was successfully employed to characterize different polymorphic and amorphous forms of other sartans (candesartan, irbesartan and losartan).[33-35]

Bauer *et al*. reported that the closely related system irbesartan exists in two different crystal structures due to tautomerism in the tetrazole ring.[33]

The focus of this study was to characterize two different amorphous forms of valsartan to provide insight into their amorphous structures and molecular mobility, employing solid-state NMR as a primary investigation tool supported by solution-state NMR, FT-IR, and TMDSC. Dissolution tests were also carried out to compare dissolution rates of the two forms.

EXPERIMENTAL SECTION

Materials

Valsartan (form AR, as-received, pharmaceutical grade) was obtained from Polpharma, Starogard Gdański, Poland and used without further treatment. The non-crystalline nature of the material was confirmed by PXRD (see Figure S1 of the Supporting Information) and the lack of birefringence when analyzed by polarizing light microscopy. We have also analyzed materials from two other suppliers (Zydus Cadila, Ahmedabad, India and Wuhan Fortuna Chemical Co. Wuhan, China) and all samples were essentially identical by DSC and TMDSC as the sample (AR) used here. Its fully amorphous form (form AM) was prepared immediately prior to experimental measurements in DSC pan in the instrument, in the NMR rotor in the probe or in an oven, by heating sample to 130–140 °C, holding for 10–20 min then cooling with at least approximately 3 °C min^{-1} cooling rate to room temperature. The purity of both AR and AM materials was verified by solution ^{1}H and ^{13}C NMR.

Attempts to obtain crystalline material by re-crystallization based on previous published reports or patents[20, 36-39] were unsuccessful.

Intrinsic and apparent dissolution testing

The Intrinsic Dissolution Rate (IDR) of both amorphous samples was measured by the rotating disc method[40] using the Wood apparatus in an Erweka DT60 dissolution testing station (ERWEKA GmbH, Germany). 150 mg of API was compressed at 1300 psi and held for 40 s in a die to form an 8 mm

diameter disc. Dissolution studies were performed in 900 mL of deionisedand deaerated water (pH = 6.9, conductivity < 0.1 μS cm^{-1}) maintained at a temperature of 37 ±0.5 °C and disk rotation speed of 100 rpm. Dissolution studies were carried out for 120 minutes and the concentration of API was determined on-line every 1 minute by a UV spectrophotometer at 250 nm (120 points). All measurements were performed in triplicates. IDR, the rate of mass transfer from solid to liquid state when conditions such as surface area, pH, ionic strength and stirring speed are kept constant, was determined using the following equation[41]:

$$\mathrm{IDR} = \frac{C}{t}\frac{V}{S} = kC_s \quad (1)$$

where C is the drug concentration at time t, V is the volume of the test solution, S is the surface area of the disc, k is intrinsic dissolution rate constant, and C_s is the saturation solubility of the drug. The IDR was calculated from slope of each curve for a time period of 0–120 min.

The apparent dissolution of both amorphous samples was measured by an on-line closed loop semi-automated flow through a cell dissolution system (SOTAX AG, Switzerland) using the Apparent Dissolution method defined in Chapter 2.9.43 of the Ph. Eur. 8.0.[42] The dissolution system consisted of: SOTAX CE 7 unit, SOTAX CP 7-35 piston pump, reservoirs for the dissolution medium (SIMAX 1 L orange glass bottles placed on magnetic stirrers with integrated temperature control plate) and double-beam UV-Vis spectrophotometer Nicolet Evolution 300 (Thermo Electron Corporation, USA). Each 12 mm diameter cell was prepared by placing a 5-mm ruby bead in the apex of the cone to protect the inlet tube, and glass beads were added to the cone area to form a bead bed. Two sieves separated by a glass microfiber filter (GF/D Whatman with a retention capacity of 2.7 μm) and 50 mg of powder to be studied were respectively placed on the top of the layer of beads. The cell was closed with the prepared insert and the filter head consisting of one sieve and a glass microfiber filter (GF/F Whatman with a retention capacity of 0.7 μm). The closed-loop configuration used a 1000 mL of deaerated ultra-pure water (pH = 6.9, conductivity < 0.1 μS cm^{-1}) per cell. Deaeration was performed using the SOTAX

Media Preparation Station. Reservoirs were placed in the line at RT-10 Power IKAMAG magnetic stirrers (IKA, Germany) allowing the medium to be stirred, heated and sampled. The medium was circulated with a constant flow rate of 8 mL min^{-1} (±2%) and maintained at 37.0 ±0.5 °C. After passing through the cell, the eluents were filtered and then transferred directly through the UV spectrometer. Measurements at 250 nm were taken in flow-through cuvettes with 10 mm path length every 1 min up to 120 min. The WinSOTAX Plus Dissolution Software automatically read the baseline for each cell, recorded raw absorbance data, corrected data, and calculated concentration and % of dissolved drug. The measuring system consisted of seven chambers, allowing six powders to be tested simultaneously, with one chamber filled only with dissolving medium (blank sample). Each sample was tested in three chambers simultaneously (n = 3) and the final results were reported as an average, with the uncertainty represented by standard deviation (±SD). The drug dissolution and release profiles were plotted as the percentage of dissolved drug as a function of time. To quantify the *in vitro* dissolution kinetics, the first-order model:

$$F(t) = F_0[1 - \exp(-k_D t)] \quad (2)$$

(where F is the fraction of drug dissolved at time t and k_D is the dissolution rate constant[43]) was fitted to the three individual dissolution profiles with linear least-squares curve-fitting technique using DDSolver software.[44]

NMR measurements

Solution-state NMR experiments were carried out on a Varian VNMRS-700 machine with ^{1}H and ^{13}C frequencies of 699.73 and 175.97 MHz respectively. Spectra of valsartan were measured in 0.5 mL of [D_6]-DMSO. All measurements were performed at 25 °C.

Carbon-13 solid-state NMR spectra were acquired using a Varian InfinityPlus spectrometer operating at a ^{13}C frequency of 125.68 MHz. A magic-angle spinning (MAS) probe using 5 mm diameter zirconia rotors was employed. Typical operating conditions used cross-polarisation (CP) for excitation of the ^{13}C magnetisation with a CP contact time of 2 ms, a recycle delay of 2 s, 512 to 2048 transients and spin rate of 6 or 10 kHz. Carbon chemical shifts were referenced to the signal for tetramethylsilane *via* a

replacement sample of solid adamantane (38.4 ppm for the high-frequency line). Variable-temperature experiments were performed from 38 °C to 110 °C, allowing samples to stabilize for 15–20 min before starting acquisition. Unless otherwise stated, temperatures in these experiments are quoted with a correction of +16 °C above the displayed temperature, which is the estimated increase in sample temperature for a 5 mm rotor spinning at 10 kHz, based on previous calibration experiments using lead nitrate.[45]

Carbon-13 T_1 relaxation times were measured with cross polarisation using the "Torchia" method,[46] although without ^{1}H decoupling during the relaxation period, using 21 recovery periods, τ, from 0.01 to 80 s, acquiring 64 transients per point. T_1 values were obtained by fitting the measured peak heights (after applying a Gaussian line broadening of 80 Hz) as function of τ to a simple mono-exponential decay. Molecular motions on the kHz time scale were probed by measuring ^{1}H *via* ^{13}C spin-lattice relaxation times in the rotating frame, $T_{1\rho}$. Spin-locking pulse lengths were varied in 20 steps from 1 to 20 ms, following a 90° radio frequency pulse (4.2 μs) and the peak heights as a function of pulse length fitted to a mono-exponential decay. The overlapped signal at 27.5 ppm showed multi-exponential character, and so was not fitted. The T_1^C values for non-protonated carbons (C-5, C-10 and C-24 carbons) were too long to measure with any precision.

Proton MAS spectra were recorded using a Varian InfinityPlus 500 spectrometer operating at a ^{1}H frequency of 499.70 MHz. A Bruker MAS probe using 1.3 mm diameter zirconia rotor was employed. Spectra were typically acquired using a recycle delay of 10 s, 64 transients and spin rate of 67 kHz. Spectra were also recorded at 43 and 53 kHz spinning rate, where frictional heating is significantly lower, gave identical results apart from lower spectral resolution. Proton broadline NMR spectra and proton relaxation times (T_1^H and $T_{1\rho}^H$) for static samples were measured at 299.82 MHz using a Varian UnityPlus spectrometer. T_1^H was measured using saturation-recovery experiments. Spectra were measured over a temperatures range from 25 to 120 °C, allowing at least 15 min for stabilization before acquisition. All measurements were performed in duplicates for two different samples. Uncertainties listed are the

standard errors in the parameters as determined from non-linear regression analysis using SigmaPlot 12.0 (Systat Software Inc.).

Nitrogen-15 solid-state NMR spectra were recorded with CP and MAS using the Varian VNMRS and the Varian InfinityPlus spectrometers, operating at ^{15}N frequencies of 40.53 and 50.65 MHz respectively, and probes taking 6 mm and 5 mm diameter rotors respectively. Typical operating conditions used a CP contact time of 5 or 10 ms, a recycle delay of 1.5 or 2 s, 40000 to 150000 transients and spin rate of 6 or 10 kHz. Nitrogen chemical shifts were referenced using ^{15}N-enriched glycine at –347.4 ppm relative to the signal of neat nitromethane. Variable-temperature experiments were performed at 38, 80 and 110 °C, allowing samples to stabilize for 15–20 min before starting acquisition. Unless otherwise stated, temperatures on the 5 mm probe and 10 kHz spinning rate are quoted with a correction of +16 °C as for the ^{13}C SSNMR experiments. Inversion-recovery (IR) CP MAS experiments were recorded with inversion time of 1 ms as described in Ref.[47]

The ^{1}H–^{13}C Heteronuclear Correlation (HETCOR) spectra were obtained at ambient temperature using the Varian VNMRS 400 spectrometer employing 4 or 6 mm rotors, with Frequency Switched Lee-Goldburg CP, two-pulse phase modulation decoupling, contact times of 0.1 and 1.0 ms, 32 increments in the indirect dimension, 288 or 512 transients, recycle delays of 2 s and a spin rate of 10 kHz. A sample of glycine was employed for calibration.

NMR data were processed using gsim[48] and ACD/Spectrus Processor (Advanced Chemistry Development Inc.). Unless stated otherwise, Gaussian line broadening of 40 Hz and 60 Hz were applied to the ^{13}C and ^{15}N spectra respectively. A "resolution enhancement" corresponding to an 80 Hz Gaussian function was applied to the ^{1}H MAS spectra.

Gauge Including Projector Augmented Wave[49, 50] calculations were carried out with the CASTEP v. 6.0 computer program[51] for the crystalline valsartan given in Ref.[20] All calculations were performed using the PBE functional[52] using on-the-fly generated ultrasoft pseudopotentials. Geometry optimisations for all atoms were carried out with the centre of mass fixed and a cut-off energy of 600 eV, with integrals taken over the Brillouin zone using a Monkhorst–Pack grid[53] with 12 k-points and the unit cell parameters

fixed to the values determined by single crystal XRD. NMR calculations used the same cut-off energy and Brillouin zone integration.

FT-IR measurements

Fourier transform infra-red spectroscopy was carried out using an Alpha Bruker FT-IR spectrometer in KBr pellets. Spectra were recorded at room temperature from 4000 to 500 cm^{-1} collecting 64 scans with a resolution of 2 cm^{-1}.

TMDSC measurements

Temperature-modulated DSC (TMDSC) curves were obtained using a DSC Q1000 TA Instrument Inc. (V9.9 Build 303) with an underlying heating rate of 3 °C min^{-1} and a temperature modulation with amplitude of 1.5 °C and period of 60 s (this is sometimes termed "standard TMDSC") from 25 to 120 °C under a nitrogen gas flow of 50 mL min^{-1}. The samples were then cooled at 25 °C min^{-1} to 20 °C without modulation and reheated to 120 °C with modulation in a second run.

The enthalpy change after isothermal physical ageing was determined as a function of ageing time. Samples were first heated to 120 °C and held for several minutes to eliminate the effect of prior thermal history and then cooled at 25 °C min^{-1} below the glass transition temperature to the ageing temperature, T_a, which was 30, 40, 50 or 60 °C. The samples were maintained at T_a for specified times ranging from 0 to 16 hrs, and then cooled at 25 °C min^{-1} to 25 °C. A subsequent heating scan at 3 °C min^{-1} by TMDSC to 120 °C provides the data for the aged samples.[54, 55] The modulation parameters were the same as above.

The equipment was calibrated with indium (*m. p.* = 156.65 °C, ΔH_f = 28.45 J g^{-1}), and at least two tests were run on each sample. Relaxation events are quoted as an onset temperature. Glass transition temperatures are quoted as midpoints. All values were determined using TA Universal Analysis 2000 V4.5A software. Errors are quoted as one standard deviation.

RESULTS AND DISCUSSION

Intrinsic dissolution rate (IDR) and apparent dissolution rate (ADR)

The dissolution profile of an API can have a profound impact on both pharmacokinetic and pharmacodynamic parameters.[56] Figure 2A shows intrinsic dissolution profiles for AR and AM valsartan in deionised water. AR valsartan showed significantly higher IDR value of 24.6 ±0.1 μg min^{-1} cm^{-2} compared to 11.0 ±0.1 μg min^{-1} cm^{-2} for the AM sample (*t*-test at $\alpha = 0.05$, $p = 0.00003$). Apparent dissolution tests of the powdered drugs in deionised water, Figure 2B, also show significant differences (*t*-test at $\alpha = 0.05$, $p = 0.00225$) between the first-order dissolution rate constants, k_D (14.3×10^{-4} min^{-1} vs 7.5×10^{-4} min^{-1} for AR and AM forms respectively). The higher free energy of amorphous materials is generally associated with increased solubility and dissolution rates.[4-6] It is, therefore, surprising to find that the fully amorphous material (AM form) has the lower dissolution rate.

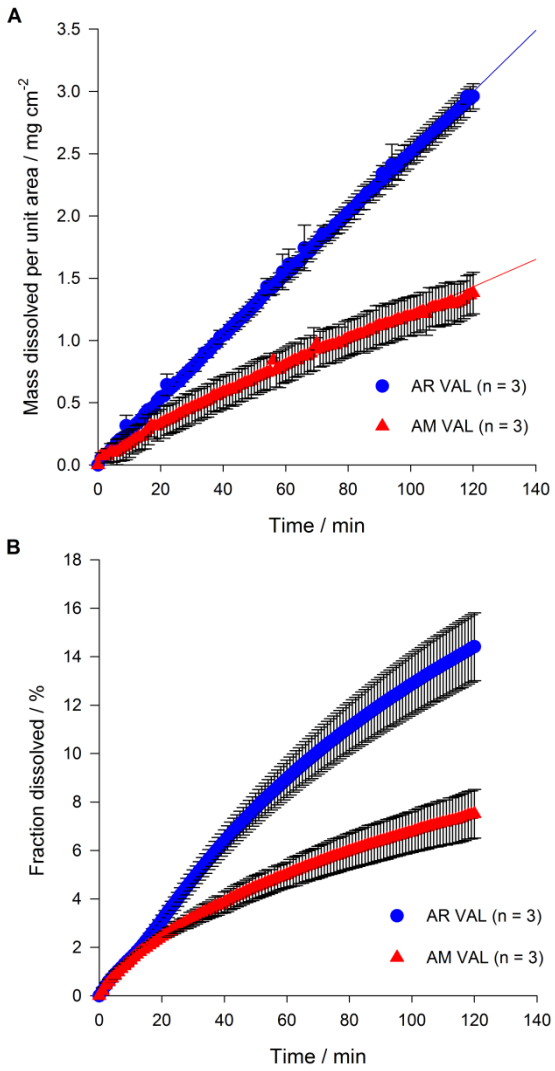

Figure 2. (A) Intrinsic and (B) apparent dissolution profiles of valsartan in different solid state forms in deionised water.

Carbon-13 SSNMR

Figure 3 shows ^{13}C CP MAS NMR spectra of the two valsartan forms. Both spectra are relatively broad, reflecting the amorphous nature of the materials as reported elsewhere (see Figure S1 of Supporting Information).[30] The resonances were assigned based on ^{13}C solution-state NMR and by computational prediction of chemical shifts based on the crystal structure of Ref.[20], although assignment is limited by peak overlap and the broadness of the resonances. Table I lists the chemical shifts for two solid-states of valsartan and compares them to corresponding solution-state and calculated values.

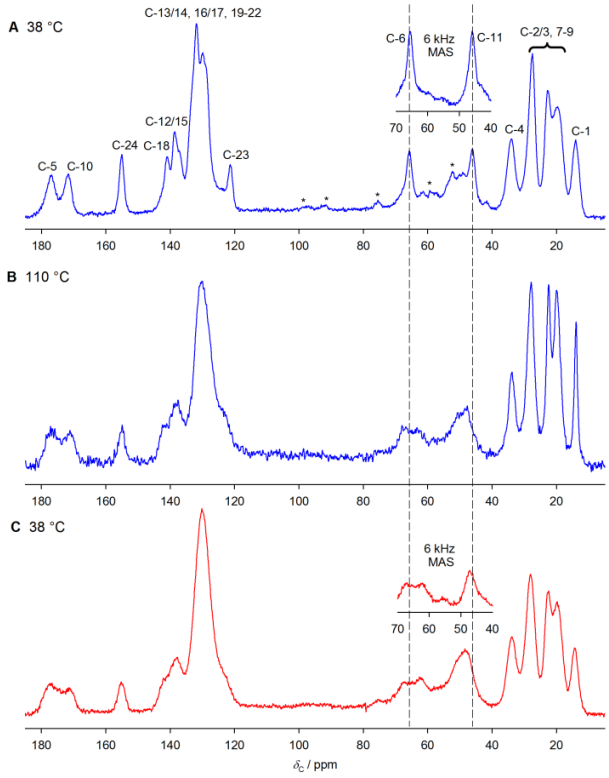

Figure 3. ^{13}C CP MAS NMR spectra of as-received valsartan (AR form) at (A) 38 °C, (B) above the glass transition temperature at 110 °C and (C) fully amorphous valsartan (AM form) at 38 °C. Spectra recorded at 10 kHz spinning rate, asterisks denote spinning sidebands. Insets show 40–70 ppm region of spectra recorded at 6 kHz spinning rate, which are less affected by spinning sidebands.

Table I Solution-, solid-state and calculated ^{13}C chemical shifts for valsartan at 25 °C (in [D_6]-DMSO) and 38 °C (solid state).

Carbon No	Solution-state NMR δ_C / ppm		Solid-state NMR δ_C / ppm		Calculated $\delta_{C(calc)}$ / ppm[a]
	Major conformer (*trans*)	Minor conformer (*cis*)	AR VAL	AM VAL	Crystalline VAL (*cis*)
1	14.16	14.25	14.1	14.3	11.8
8	18.25	18.93	19.8 22.6 27.6	19.8 22.6 28.0	22.3
2	22.12	22.27			24.7
9	20.59	19.84			25.2
3	27.26	27.45			27.9
7	28.00	28.04			29.8
4	32.90	32.94	34.1	33.8	34.3
11	49.15	45.90	46.2	48.3	51.2
6	63.39	66.18	65.8	62.3, 67.3	73.1
23	123.50[b]	123.50[b]	121.3	123 – 139 with maxima at 130.1 138.0	129.7
19	130.98	131.05	123 – 139 with maxima at 129.7 131.8 138.5		135.5
21	128.14	128.01			136.2
16	129.24	128.73			136.2
14	129.24	128.73			136.9
13	126.72	127.37			137.4
17	126.72	127.37			138.5
20	130.98	131.05			139.0
22	131.51	131.51			142.7
12	138.22	137.55			143.9
15	138.22	138.67			145.2
18	141.65	141.78	140.8	141.9	150.4
24	155.00[b]	155.00[b]	155.1	155.1	166.1
10	172.34	172.07	171.7	171.3	180.6
5	173.91	173.88	176.8	177.3	181.8

[a] $\delta_{C(calc)} = \sigma_{ref} - \sigma_{calc}$ where $\sigma_{ref} = 176.1$ ppm cf. Figure S2A of Supporting Information.
[b] Not observed. Data taken from Ref.[57], acquired in 1:1 [D_6]-DMSO/D_2O solution

The main difference between AR and AM spectra is for carbons directly bonded to the amide nitrogen (N-1) i.e. C-11 and C-6. In the fully amorphous material, the C-11 signal is broadened and at higher chemical shift ($\Delta\delta_C$ = +2.1 ppm). The C-6 resonance at 65.8 ppm in the AR spectrum is split into two broad signals with maxima at 62.3 and 67.3 ppm in the AM form spectrum (clearer in the insets acquired at 6 kHz MAS rate in Figure 3C). The ^1H–^{13}C HETCOR spectrum also clearly showed a pair of cross-peaks from C-6 in the AM form (Figure S3, Supporting Information). Valsartan in solution exists in two conformations (*cis–trans*) due to restricted rotation around the C(O)–N amide bond,[21, 57] cf. Figure 1. Significant differences can be observed for C-11 and C-6 solution-state chemical shifts for *cis* and *trans*

conformers (for C-11, δ_C^{cis} = 45.90, δ_C^{trans} = 49.15 ppm and for C-6, δ_C^{cis} = 66.18, δ_C^{trans} = 63.39 ppm), where the *cis* vs *trans* assignment was made on the basis of NOESY experiments. These indicated that *trans* conformation is favoured in DMSO solution, while the *cis* conformation is exclusively occupied in the only known crystal structure.[20] The splitting of the C-6 signal and broadening of the C-11 signal in solid-state NMR experiments suggests that AM form of valsartan contains an approximately equal ratio of *cis* and *trans* conformers. Care is required when comparing chemical shifts between solid and solution states. However, the trend line for computed chemical shifts from the known solid-state form (*cis* conformation), Figure S2 of Supporting Information, is a better fit for the ^{13}C solution-state shifts of the *cis* rather than *trans* conformation. Taken together with the excellent agreement of the AR form shifts with the *cis* solution-state shifts, this strongly suggests that the AR form involves the *cis* isomer. In contrast to the aliphatic region below 40 ppm, the signals at higher frequency, from the phenyl rings, the carbon in the tetrazole ring (C-24), the amide and acid carbons (C-5, C-10), all broaden significantly in the AM spectrum.

Heating both materials above the glass transition results in indistinguishable ^{13}C NMR spectra, Figure 3B (full results shown in Figures S4 and S5 of the Supporting Information), showing that both starting materials have "relaxed" to the same form. The aliphatic peak linewidths (C-1–C-4 and C-7–C-9) are noticeably sharper at 110 °C, which corresponds to increased molecular mobility. In contrast there is little narrowing of the aromatic region, implying that the mobility of the alkyl regions is local rather than affecting the molecules as a whole. Equalisation of the *cis* vs *trans* distribution has occurred for the AR form during its glass transition. Similar behaviour for an API, captopril, containing amide bond but in an initially crystalline form, was observed during melting of an initially crystalline material by Wang *et. al.* using VT FT-IR microscopy.[58] Similarly amide *cis–trans* interconversion in the solid state was postulated as the origin of polymorphism in fosinopril sodium using SSNMR and FT-IR.[59]

^{1}H solid-state NMR

Wideline (static) ^{1}H NMR spectra of the two forms as a function of temperature are very similar, and show the expected narrowing of NMR spectrum above the glass transition as a result of increased mobility, cf. Figure S6 of the Supporting Information. ^{1}H spectra acquired under ultra-fast magic-angle spinning to reduce the line-broadening associated with the strong dipolar interactions between ^{1}H spins are more informative. As shown in Figure 4, five resonances are clearly distinguished in the spectrum of as-received valsartan, corresponding to alkyls (≈0.9 ppm), alkyls bonded with N-1 (≈5.6 ppm), aromatic (≈7.1 ppm), acidic (≈14.2 ppm) and tetrazole (≈16.4 ppm) protons. The C-6 and C-11 signals are not resolved for the amorphous form. The assignment of the high frequency signals was based on the CASTEP-predicted ^{1}H shifts using the crystal structure of valsartan given by Wang *et al.* (Figure 1B);[20] the calculated shielding is +2.4 ppm higher for the acidic proton compared to the tetrazole, which is a good match for the experiment shift difference of –2.2 ppm (accounting for the opposite directions of shielding and chemical shift scales). In this structure, valsartan molecules are connected *via* two hydrogen bonds, both associated with the tetrazole ring: one between the carboxylic acid group (C-10) and N-2, and the other one between the carbonyl group (C-5) and N-5. The ^{1}H MAS experiments are consistent with the tetrazole (N(5)H) and acidic (C(10)OOH) protons being involved in similar hydrogen bonding arrangements in the crystalline and AR forms. In contrast, the ^{1}H spectrum of the fully amorphous form shows a single very broad feature in this region implying a much wider distribution of hydrogen bonding environments in the AM form.

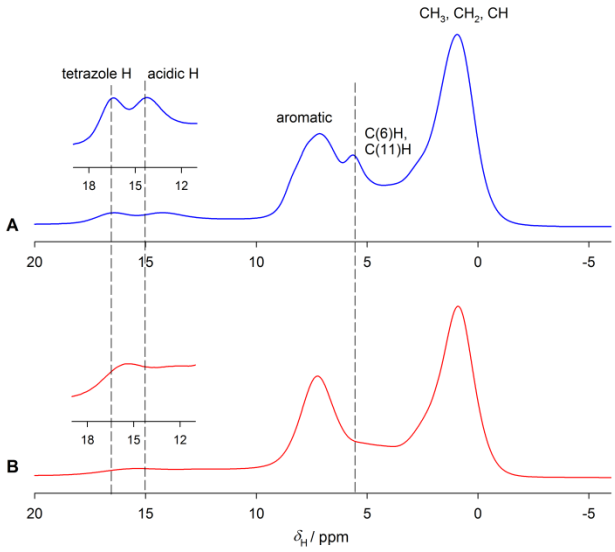

Figure 4. ^{1}H MAS NMR spectra of (A) as-received (AR form) and (B) fully amorphous (AM form) valsartan recorded at a MAS rate of 67 kHz.

Nitrogen-15 SSNMR

Solid-state ^{15}N CP MAS NMR has been successfully employed to examine polymorphism of a closely related system, irbesartan.[33] Like irbesartan, valsartan can potentially exist in two tautomeric forms of the tetrazole ring i.e. as 1,2,3,4-tetrazole or 1,2,3,5-tetrazole as presented in Figure 5A. Figure 5B–E shows ^{15}N CP MAS NMR spectra of both valsartan forms. The spectrum of the as-received material, Figure 5B, has the expected five strong signals (tetrazole + amide nitrogen), but also weak signals at about –52, –160 and –255 ppm. The spectrum of the AM form shows broader signals in the same positions, but these smaller signals are significantly stronger. Assignments are made by comparison with literature ^{15}N data for tetrazole-containing systems, computational prediction of chemical shifts for crystalline valsartan, and experimental determination of the protonation site. ^{15}N dipolar dephasing experiments were unsuccessful, presumably because the ^{15}N,^{1}H dipolar couplings are too strongly affected by the magic-angle spinning required for site resolution,[60] but the inversion recovery CP MAS experiment,[47] Figure 5E, clearly identified the signal at –149.4 ppm as the protonated nitrogen. As seen in Table II and Figure S2B of the Supporting Information, the assignment is excellent agreement with the computational prediction of

chemical shifts for crystalline valsartan and is in much better agreement with the 1,2,3,4-tetrazole tautomer of irbesartan (form A) rather than the 1,2,3,5-tetrazole (form B). Hence we can conclude that both AR and AM forms of valsartan exist as a 1,2,3,4-tetrazole tautomer. The significantly better agreement of the computed shieldings of the crystalline form (*cis* conformer) with the strong peaks of the AR form again suggests that the strong peaks correspond to the *cis* conformer. The additional weak signals in the AR form, which are stronger in the AM form, are likely to correspond to the *trans* conformer. The crowded nature of the spectrum means that the weak peaks from the minor conformer cannot be confidently identified in the ^{13}C spectrum of the AR form, although the spectrum is clearly not inconsistent with their presence.

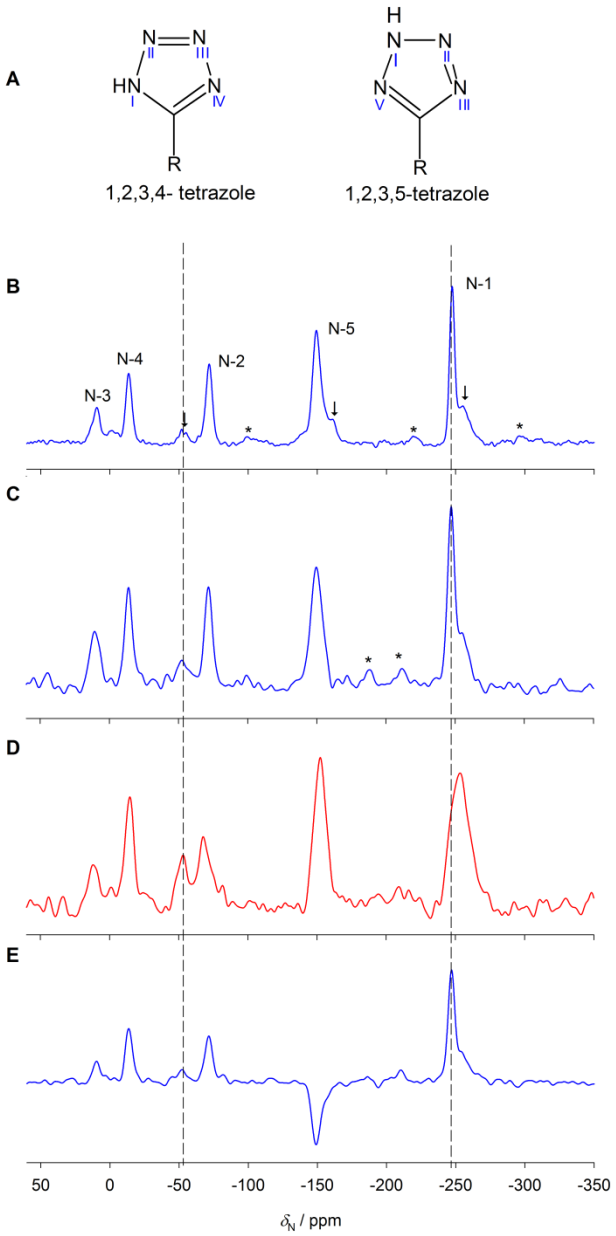

Figure 5. (A) Possible tautomeric forms of valsartan: 1,2,3,4- and 1,2,3,5- forms. ^{15}N CP MAS NMR spectra of AR VAL (B) at 6 kHz spinning rate (151 000 repetitions in total) (C) at 10 kHz spinning rate (30 000 repetitions in total), (D) AM VAL at 10 kHz spinning rate (40 000 repetitions) and (E) ^{15}N IR CP MAS NMR spectrum of AR VAL at 10 kHz spinning rate (331 000 repetitions in total). Arrows (↓) indicate signals from isomeric impurity in the AR form. (B) was acquired at 40.53 MHz and other spectra at 50.65 Mz. All spectra recorded at room temperature. Asterisks (*) denote spinning sidebands. Note N-(I–IV) in diagram A correspond to N-(5–2) in figure B, respectively.

Table II Nitrogen-15 chemical shifts for valsartan and other related tetrazole systems.

Compound	δ_N / ppm					Ref.
	N-I[a]	N-II[a]	N-III[a]	N-IV[a]	N amide	
Major conformer in AR valsartan[b] (1,2,3,4-tetrazole)	–149.4, (N-5)	–13.2 (N-4)	10.3 (N-3)	–71.2 (N-2)	–247.3 (N-1)	this work
Minor conformer in AR valsartan[b] (1,2,3,4-tetrazole)	–160.3 (N-5)	–[c]	–[c]	–51.7 (N-2)	–254.9 (N-1)	this work
Minor/major conformers in AM valsartan[b] (1,2,3,4-tetrazole)	–152.5 (N-5)	–15.2 (N-4)	11.5 (N-3)	–53.6, –67.8 (N-2)	–253.3 (N-1)	this work
Cis crystalline valsartan (calculated)[b,d] (1,2,3,4-tetrazole)	–149.0 (N-5)	–18.4 (N-4)	13.8 (N-3)	–68.1 (N-2)	–244.1 (N-1)	this work
Irbesartan form A (1,2,3,4-tetrazole)	–143.4	–13.6	13.0	–54.2	–216.4	this work
5-phenyltetrazole (1,2,3,4-tetrazole)	–153.2	–16.9	5.1	–78.0	–	[33]
Irbesartan form B[e] (1,2,3,5-tetrazole)	–79.3 (N-24)	–88.7 (N-25)	–3.2 (N-26)	–50.7 (N-27)	–219.0[f]	[33]

[a]Nitrogen atom labelling is the 1,2,3,4-tetrazole convention as in Figure 5A.
[b]Labels in parentheses are those used in this work and Ref.[20]
[c]Signals not resolved.
[d]$\delta_{iso} = \sigma_{ref} - \sigma_{iso}$, where σ_{ref} = –164.9 ppm (Figure S2B, Supporting Information).
[e]Labels in parentheses are those used in Ref.[33]
[f]Values originally reported with respect to nitrate resonance of solid external ammonium nitrate but here reported relative to nitromethane for consistency.

Fourier transform infra-red spectroscopy (FT-IR)

FT-IR measurements revealed only subtle differences between the two forms, cf. Figure S7 of the Supporting Information. AR valsartan shows absorption bands at 1732.1 cm^{-1} and 1603.8 cm^{-1}, assigned to carboxyl carbonyl (C-10) and amide carbonyl (C-5) stretching vibrations respectively, that are potentially sensitive to changes in hydrogen bonds. There was, however, no change in the AM form in the carboxyl carbonyl band (1732.1 cm^{-1}), while the C-5 carbonyl peak shifted towards higher wavenumber (1605.8 cm^{-1}). This is consistent with the differences in the forms relating to *cis–trans* conformational changes, although changes in the intermolecular hydrogen bonds between C(5)O and the tetrazole N(5)H group could also be a factor. As well as minor changes in the fingerprint region (inset of Figure S7), there is some attenuation of the broad peak centred about 3436 cm^{-1} (N(5)H and/or OH) which is likely to reflect changes in hydrogen bonding.

Molecular mobility from NMR relaxation times

Variable-temperature, wideline (static) ^{1}H spin-lattice relaxation time, T_1^{H}, experiments provide information on molecular mobility of both forms. T_1^{H} is sensitive to motional processes of the order of the ^{1}H NMR frequency,[25] here 300 MHz, and is typically sensitive to high-frequency local motions. The T_1^{H} measurements show a monotonic increase in the T_1 values with increasing temperature for both forms (Figure 6A), consistent with frequency of local motions increasing into the GHz range above ambient temperature. This increase is smooth through T_g, suggesting that the local motions are not significantly affected by the glass transition.[23, 61] The values of T_1^{H} are measurably different for the two forms at room temperature, but converge, as might be expected, as the glass transition is approached.

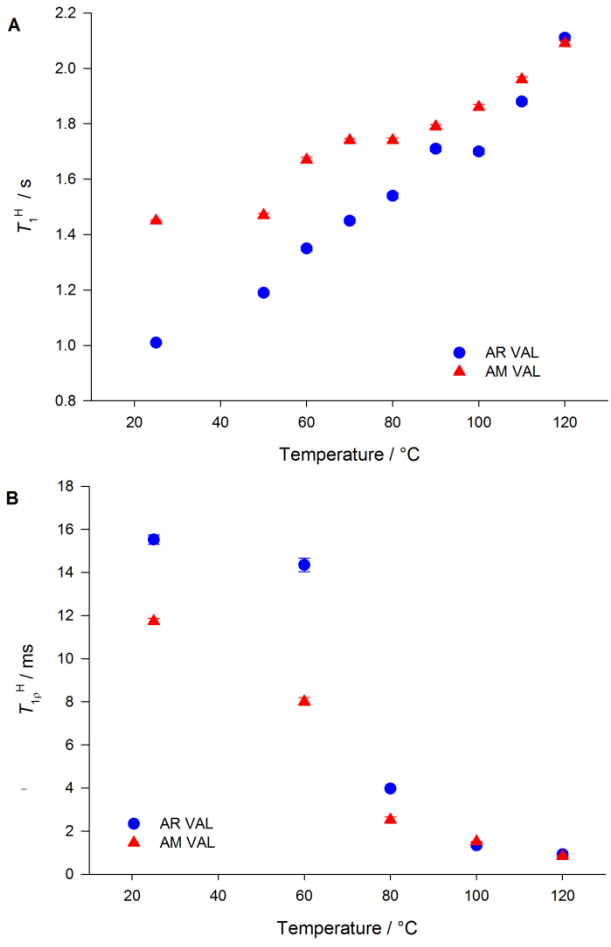

Figure 6. Static proton (A) T_1 and (B) $T_{1\rho}^{H}$ data for AR and AM valsartan forms.

Wideline measurements of T_1^H provide an overview of high-frequency local motions which can be refined by measurements of ^{13}C T_1 relaxation times (at the expense of greatly increased experimental time), since these provide information on site-specific dynamics. The detailed values are given in Table SI of the Supporting Information and the results for characteristic carbons are shown in Figure 7. The relaxation behaviour of the aliphatic carbons of the butyl chain (C-1–C-3) and the isobutyl group, Figure 7A–C, is very similar and essentially identical between forms. The temperature dependence of the dynamics driving the relaxation can be fitted by plotting the relaxation times as a function of the inverse of the temperature. This dependence can be interpreted, in terms of empirical activation barriers of the order of 8–12 kJ mol^{-1} (Figure S8, Supporting Information). Note how the major changes in bulk molecular mobility associated with the glass transition are not apparent from these relaxation times. In contrast, the aromatic carbons have relatively long relaxation times at ambient temperature which drop significantly at the glass transition, Figure **7**E. This change is smooth for the truly amorphous material, but there is some evidence of a more step-like behaviour for the AR material. This suggests that the glass transition is associated with an "unlocking" of the aromatic rings. The relaxation time of C-4, Figure 7D, behaves somewhat differently to that of the other aliphatic carbons, which is consistent with amide group having different motional character to the alkyl chain and isobutyl group.

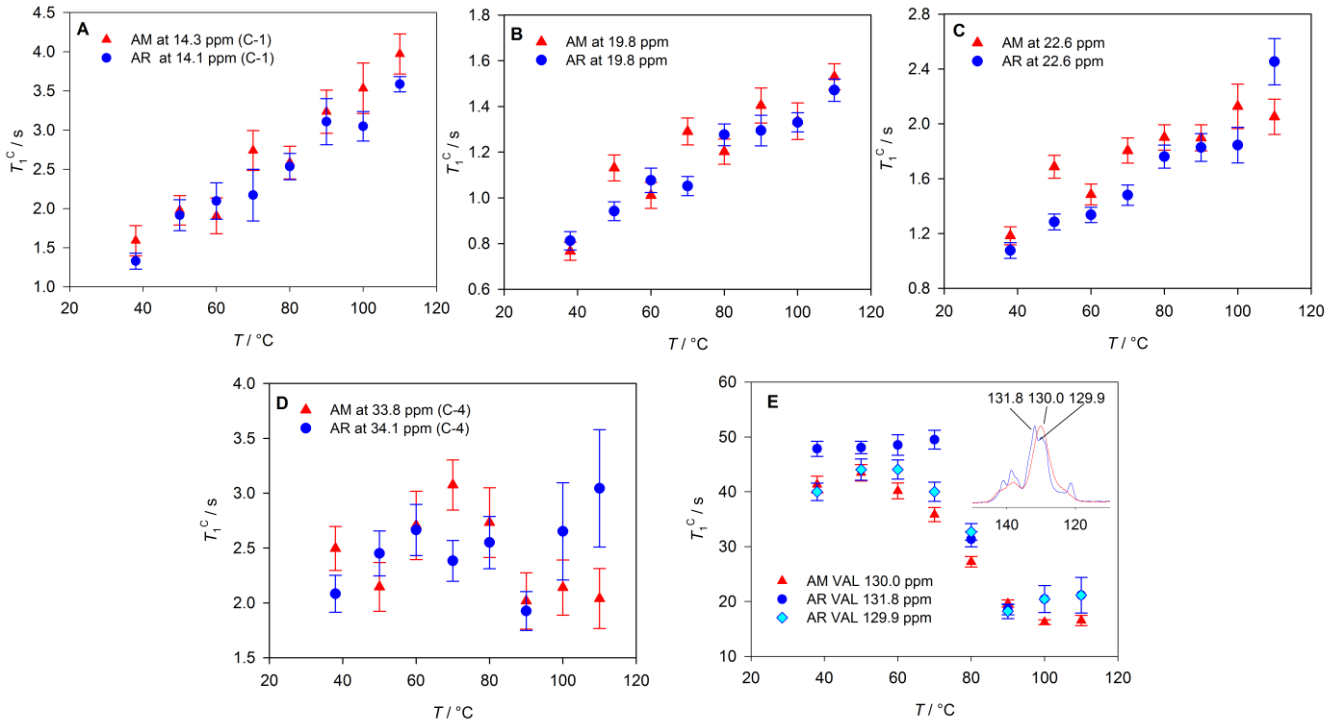

Figure 7. ^{13}C T_1 relaxation time constants of AR and AM valsartan forms as a function of temperature for (A–D) aliphatic and (E) aromatic carbons.

The ^{1}H $T_{1\rho}$ relaxation time is sensitive to motion on the order of the RF nutation rates,[25] here 125 kHz. Such slower processes are often associated with bulk mobility rather than the local high-frequency motions probed by spin-lattice relaxation times. The $T_{1\rho}{}^{H}$ as a function of temperature were obtained for the two forms of valsartan from wideline measurements, Figure 6B. The $T_{1\rho}{}^{H}$ values for the AR material below the glass transition are higher than for totally amorphous valsartan, but converge above T_g. These differences are much smaller than those typically observed between amorphous and truly crystalline materials.[24] Experiments to measure site-specific ^{1}H $T_{1\rho}$ values by transferring the partially relaxed ^{1}H magnetisation to ^{13}C *via* cross-polarisation prior to measurement were relatively uninformative, showing uniform behaviour across sites, cf. Figure S9 and Table SII of Supporting Information, although again a more step-like character to the temperature dependence was observed for the AR material. Spin-diffusion between ^{1}H will tend to equalise $T_{1\rho}{}^{H}$ values, which may, in any case, be probing overall bulk mobility rather than site-specific motions.

The effect of annealing on the AM form

During physical ageing amorphous materials lose excess enthalpy as they evolve towards more stable arrangements. This enthalpy loss is recovered by the system during the heating DSC step and is measured as an integral of enthalpy recovery peak, which overlaps with a change of heat capacity at glass transition on standard DSC. Such enthalpy relaxation reflects the molecular mobility in the glassy state.[62] The impact of annealing at different temperatures below the glass transition was investigated by temperature-modulated DSC. By imposing a time-dependent modulation on the temperature ramp, TMDSC decomposes the overall heat flow in a reversing (thermodynamic) and non-reversing (kinetic) heat-flow or heat capacity signal.[54] Figure 8 shows the TMDSC traces for AM valsartan annealed at 50 °C for different periods. The enthalpy recovery peaks on the non-reversing curve, Figure 8C, increase and shift to higher temperatures as ageing time increases. Only the glass transition is observed on the reversing curve. This moves to higher temperature as ageing time increases. For example, T_g changes from 76.7 to 77.3 °C, the onset of enthalpy relaxation peak from 67.4 to 70.4 °C and ΔH from 2.8 to 7.4 J g^{-1} after 16 h of annealing at 50 °C. For comparison, the glass transition of AR valsartan sample is 94.4 °C, and the onset of the enthalpy relaxation peak is 91.6 °C with ΔH = 15.8 J g^{-1}. These results are consistent with the sample moving towards a more stable conformation during ageing, possibly towards conformational distribution of the AR form. The effect of annealing can still be clearly observed for samples annealed at 40 °C, but is relatively low for samples annealed at 30 °C, Figure 9. It should be noted that the observed glass transition temperature is a function of the experimental cooling rate and thermal history of glassy materials,[62] and so the values reported for valsartan determined by standard DSC and TMDSC do vary; the key information is contained in the relative changes of T_g. None of the measured TMDSC curves showed exothermic and/or endothermic behaviour due to crystallisation and melting, confirming the stability of amorphous valsartan.

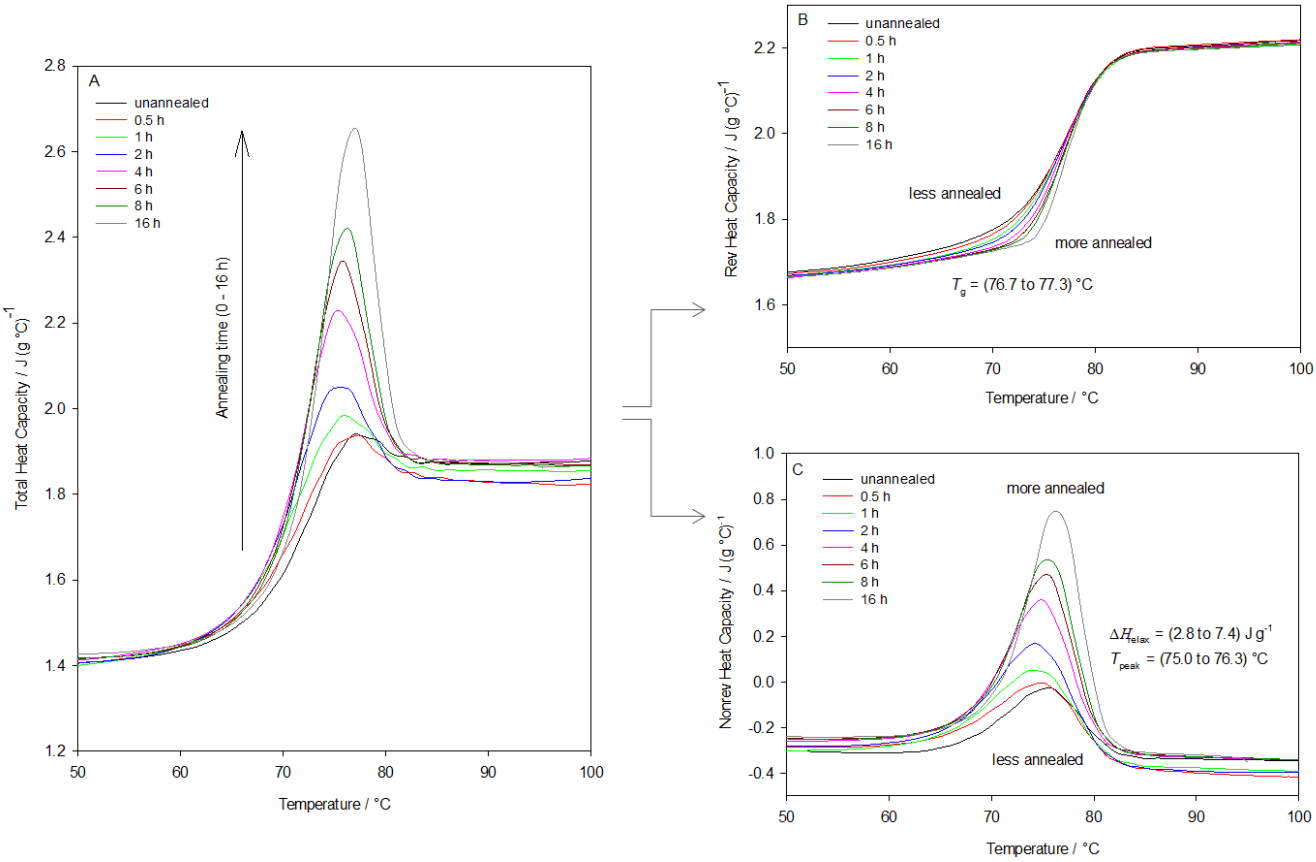

Figure 8. (A) Change of total, (B) reversing and (C) non-reversing heat capacity of AM valsartan annealed at 50 °C for different lengths of time from 0 to 16 hours.

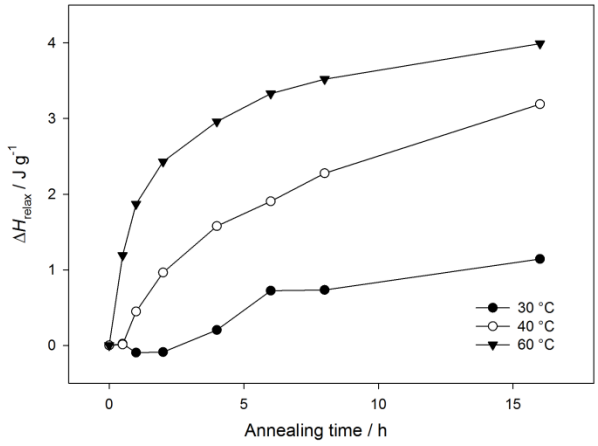

Figure 9. Enthalpy lost with time on structural relaxation of AM valsartan annealed at 30, 40 and 60 °C. The value of enthalpy relaxation at T_a = 0 h was subtracted from values of enthalpies of annealed samples to exclude effect of thermal history during cooling/heating scan. The relative standard deviations of enthalpy measurements were less than 10%. Lines drawn between points are guides for the eye.

As summarised in Table III, wideline T_1^H and $T_{1\rho}^H$ relaxation times were measured for an AM sample annealed at 60 °C, i.e. 24 °C below T_g (as determined by standard DSC). Although the changes in relaxation times are relatively small compared to the experimental uncertainties, both T_1^H and $T_{1\rho}^H$ values tend towards those of the AR material with increased annealing time. This is consistent with the mobility behaviour of the amorphous material evolving towards that of the AR material as a result of annealing. T_1^C relaxation times were measured for the annealed material, but the poorer signal-to-noise ratio in these experiments meant that any variations were too small to be observed. Similarly, changes in the ^{13}C spectrum on annealing were too small to be observed. Note that no significant changes were observed by TMDSC after ageing of the AR sample at 60 °C for up to 16 hours.

Table III T_1^H and $T_{1\rho}^H$ relaxation times for fully amorphous valsartan form (AM) as a function of annealing time. Relaxation times for AR form shown for comparison. Uncertainties listed are the standard errors in the parameters as determined from nonlinear regression analysis.

Annealing time / h	**T_1^H / s**		**$T_{1\rho}^H$ / ms**	
	AR	**AM**	**AR**	**AM**
0	0.97 ±0.004	1.53 ±0.007	14.86 ±0.21	11.64 ±0.11
1	N/A	1.28 ±0.027	N/A	11.69 ±0.16
3		1.33 ±0.009		11.48 ±0.13
19		1.25 ±0.014		12.26 ±0.18

CONCLUSIONS

The molecular structures and mobility of two solid-state forms of valsartan were investigated by solid-state NMR supported by solution-state NMR, FT-IR, TMDSC and dissolution testing. The two amorphous forms are found to be clearly distinct, with a significantly higher level of structural arrangement in the AR form, as observed in ^{13}C and ^{15}N NMR. Significant differences are noticed in the resonances from carbons directly bonded to amide nitrogen (N-1), which together with the ^{15}N NMR, suggests that the fully amorphous material contains an approximate equal ratio of *cis–trans* conformers, whereas AR form contains mainly one conformer, most likely *cis* (as in the crystalline state), with some small fraction of the other conformer. FT-IR experiments showed subtle differences which are consistent

with these observations. Further differences between both forms were observed by ^{1}H ultra-fast MAS NMR. The signals from protons bonded to C-6 and C-11 are broadened in the AM material due to amorphisation and changes in the *cis–trans* distribution, while changes in the high-frequency signals are consistent with significant differences in the hydrogen bonding involving the tetrazole and acid hydrogens. Nitrogen-15 NMR experiments confirmed that both forms exist as the 1,2,3,4-tetrazole tautomer. NMR relaxation times show subtle differences in local and bulk molecular mobility between both forms, which can be connected with the glass transition, the stability of the glassy material and its response to ageing.

Both intrinsic and apparent dissolution profiles show significant differences in dissolution kinetics for examined amorphous solid-states of valsartan. As amorphous materials have higher free energy, they usually have a greater solubility and dissolution rate than corresponding crystalline forms. Surprisingly, the less ordered, fully amorphous material (AM) has significantly *lower* dissolution rate than the apparently more ordered AR material. The results demonstrate that the method of preparation of amorphous valsartan can have a significant impact on its dissolution behaviour. These differences in dissolution rate are probably associated with the differences in hydrogen-bonding arrangements observed *via* ^{1}H NMR.

Careful characterisation of amorphous APIs is crucial, due to their generally low chemical and physical stability. Approved by US Food and Drug Administration in 1996, valsartan has so far been marketed in an amorphous form; a highly crystalline form was only obtained and patented relatively very recently. Our studies help to understand both the difficulty in obtaining crystalline forms of valsartan and the existence and stability of different amorphous forms. The flexibility of the alkyl chain and the high barrier to conformational exchange about the amide bond are impediments to forming an ordered crystal lattice, with the difficulty of conformational exchange in the solid state allowing “defects” to be easily trapped, despite the enthalpic benefits of denser packing in the AR / annealed materials. This would both explain the stable nature of the truly amorphous AM form, as well as the existence of more ordered, but still non-crystalline materials formed when solutions of valsartan are “crystallised” from solution.[29]

Solid-state NMR, in conjunction with complementary methods, such as TMDSC, allows the molecular origins of the disorder in these materials to be probed. This in turn facilitates the design of future APIs, either to deliberately stabilise amorphous materials, or to avoid the risks of poorly crystalline forms.

ACKNOWLEDGMENTS

The authors would like to thank Ms Kinga Hyla (Poznań University of Medical Sciences) for her assistance with dissolution studies and Dr Martin Dračínský (Academy of Sciences, Prague) for help with CASTEP calculations. Also, the authors acknowledge Polpharma SA Company (Starogard Gdański, Poland) for supplying valsartan used in this study.

SUPPORTING INFORMATION

Supporting Information mentioned in the main text: X-ray diffractograms of AR and AM forms of valsartan; plots of ^{13}C and ^{15}N calculated chemical shielding crystalline valsartan vs experimental chemical shifts; HETCOR spectra; VT ^{13}C CP MAS, ^{13}C direct-excitation and static ^{1}H NMR spectra; FT-IR spectra; T_1^C data as a function of reciprocal temperature and corresponding activations energies; plots of $T_{1\rho}^H$ measured *via* CP onto ^{13}C as a function of temperature; ^{13}C T_1 and $T_{1\rho}$ time constants as a function of temperature. This material is available free of charge *via* the Internet at http://pubs.acs.org.

REFERENCES

(1) Volpe, M. Preventing cardiovascular events with angiotensin II receptor blockers: a closer look at telmisartan and valsartan. *Expert Rev. Cardiovasc. Ther*. **2012,** *10*, (8), 1061-72.

(2) Shalaev, E.; Zografi, G., The concept of "structure" in amorphous solids from the perspective of the pharmaceutical sciences. In *Amorphous Food and Pharmaceutical Systems*, Levine, H., Ed. The Royal Society of Chemistry: Cambridge, 2002; pp 11-30.

(3) Petit, S.; Coquerel, G., The Amorphous State. In *Polymorphism: in the Pharmaceutical Industry*, Hilfiker, R., Ed. Wiley-VCH Verlag GmbH & Co. KGaA: Weinheim, 2006; pp 259-285.

(4) Hancock, B. C.; Parks, M. What is the True Solubility Advantage for Amorphous Pharmaceuticals? *Pharm. Res.* **2000,** *17*, (4), 397-404.

(5) Babu, N. J.; Nangia, A. Solubility Advantage of Amorphous Drugs and Pharmaceutical Cocrystals. *Cryst. Growth Des.* **2011,** *11*, (7), 2662-2679.

(6) Craig, D. Q. M.; Royall, P. G.; Kett, V. L.; Hopton, M. L. The relevance of the amorphous state to pharmaceutical dosage forms: glassy drugs and freeze dried systems. *Int. J. Pharm.* **1999,** *179*, (2), 179-207.

(7) Brittain, H. G., *Polymorphism in pharmaceutical solids*. Informa Healthcare: New York, 2009.

(8) Morris, K. R.; Griesser, U. J.; Eckhardt, C. J.; Stowell, J. G. Theoretical approaches to physical transformations of active pharmaceutical ingredients during manufacturing processes. *Adv. Drug Deliv. Rev.* **2001,** *48*, (1), 91-114.

(9) Vippagunta, S. R.; Brittain, H. G.; Grant, D. J. W. Crystalline solids. *Adv. Drug Deliv. Rev.* **2001,** *48*, (1), 3-26.

(10) Rodriguez-Spong, B.; Price, C. P.; Jayasankar, A.; Matzger, A. J.; Rodriguez-Hornedo, N. General principles of pharmaceutical solid polymorphism: a supramolecular perspective. *Adv. Drug Deliv. Rev.* **2004,** *56*, (3), 241-74.

(11) Brus, J.; Urbanova, M.; Sedenkova, I.; Brusova, H. New perspectives of ^{19}F MAS NMR in the characterization of amorphous forms of atorvastatin in dosage formulations. *Int. J. Pharm.* **2011,** *409*, (1–2), 62-74.

(12) Savolainen, M.; Heinz, A.; Strachan, C.; Gordon, K. C.; Yliruusi, J.; Rades, T.; Sandler, N. Screening for differences in the amorphous state of indomethacin using multivariate visualization. *Eur. J. Pharm. Sci.* **2007,** *30*, (2), 113-23.

(13) Patterson, J. E.; James, M. B.; Forster, A. H.; Lancaster, R. W.; Butler, J. M.; Rades, T. The influence of thermal and mechanical preparative techniques on the amorphous state of four poorly soluble compounds. *J. Pharm. Sci.* **2005,** *94*, (9), 1998-2012.

(14) Graeser, K. A.; Strachan, C. J.; Patterson, J. E.; Gordon, K. C.; Rades, T. Physicochemical Properties and Stability of Two Differently Prepared Amorphous Forms of Simvastatin. *Cryst. Growth Des.* **2008,** *8*, (1), 128-135.

(15) Ohta, M.; Buckton, G. A study of the differences between two amorphous spray-dried samples of cefditoren pivoxil which exhibited different physical stabilities. *Int. J. Pharm.* **2005,** *289*, (1–2), 31-38.

(16) Mishima, O.; Calvert, L. D.; Whalley, E. "Melting ice" I at 77 K and 10 kbar: a new method of making amorphous solids. *Nature* **1984,** *310*, (5976), 393-395.

(17) Grimsditch, M. Polymorphism in Amorphous SiO_2. *Phys. Rev. Lett.* **1984,** *52*, (26), 2379-2381.

(18) Aasland, S.; McMillan, P. F. Density-driven liquid-liquid phase separation in the system AI_2O_3-Y_2O_3. *Nature* **1994,** *369*, (6482), 633-636.

(19) Hancock, B. C.; Shalaev, E. Y.; Shamblin, S. L. Polyamorphism: a pharmaceutical science perspective. *J. Pharm. Pharmacol.* **2002,** *54*, (8), 1151-1152.

(20) Wang, J.-R.; Wang, X.; Lu, L.; Mei, X. Highly Crystalline Forms of Valsartan with Superior Physicochemical Stability. *Cryst. Growth Des.* **2013,** *13*, (7), 3261-3269.

(21) Li, F.; Zhang, H.; Jiang, L.; Zhang, W.; Nie, J.; Feng, Y.; Yang, M.; Liu, M. Dynamic NMR study and theoretical calculations on the conformational exchange of valsartan and related compounds. *Magn. Reson. Chem.* **2007,** *45*, (11), 929-936.

(22) Geppi, M.; Mollica, G.; Borsacchi, S.; Veracini, C. A. Solid-State NMR Studies of Pharmaceutical Systems. *Appl. Spectrosc. Rev.* **2008,** *43*, (3), 202-302.

(23) Apperley, D. C.; Forster, A. H.; Fournier, R.; Harris, R. K.; Hodgkinson, P.; Lancaster, R. W.; Rades, T. Characterisation of indomethacin and nifedipine using variable-temperature solid-state NMR. *Magn. Reson. Chem.* **2005,** *43*, (11), 881-92.

(24) Gao, P. Characterization of three crystalline forms (VIII, XI, and XII) and the amorphous form (V) of delavirdine mesylate using ^{13}C CP/MAS NMR. *Pharm. Res.* **1998,** *15*, (9), 1425-33.

(25) Carignani, E.; Borsacchi, S.; Geppi, M. Detailed characterization of the dynamics of ibuprofen in the solid state by a multi-technique NMR approach. *ChemPhysChem* **2011,** *12*, (5), 974-81.

(26) Luthra, S. A.; Hodge, I. M.; Pikal, M. J. Investigation of the impact of annealing on global molecular mobility in glasses: Optimization for stabilization of amorphous pharmaceuticals. *J. Pharm. Sci.* **2008,** *97*, (9), 3865-3882.

(27) Luthra, S. A.; Pikal, M. J.; Utz, M. Solid state ^{13}C NMR investigation of impact of annealing in lyophilized glasses. *J. Pharm. Sci.* **2008,** *97*, (10), 4336-46.

(28) Abdul-Fattah, A. M.; Dellerman, K. M.; Bogner, R. H.; Pikal, M. J. The effect of annealing on the stability of amorphous solids: chemical stability of freeze-dried moxalactam. *J. Pharm. Sci.* **2007,** *96*, (5), 1237-50.

(29) Tran, T. T.; Tran, P. H.; Park, J. B.; Lee, B. J. Effects of solvents and crystallization conditions on the polymorphic behaviors and dissolution rates of valsartan. *Arch. Pharm. Res.* **2012,** *35*, (7), 1223-30.

(30) Skotnicki, M.; Gawel, A.; Cebe, P.; Pyda, M. Thermal behavior and phase identification of Valsartan by standard and temperature-modulated differential scanning calorimetry. *Drug Dev. Ind. Pharm.* **2013,** *39*, (10), 1508-14.

(31) Harris, R. K. Applications of solid-state NMR to pharmaceutical polymorphism and related matters. *J. Pharm. Pharmacol.* **2007,** *59*, (2), 225-239.

(32) Tishmack, P. A.; Bugay, D. E.; Byrn, S. R. Solid-state nuclear magnetic resonance spectroscopy—pharmaceutical applications. *J. Pharm. Sci.* **2003,** *92*, (3), 441-474.

(33) Bauer, M.; Harris, R. K.; Rao, R. C.; Apperley, D. C.; Rodger, C. A. NMR study of desmotropy in Irbesartan, a tetrazole-containing pharmaceutical compound. *J. Chem. Soc., Perkin Trans. 2* **1998**, (3), 475-482.

(34) Raghavan, K.; Dwivedi, A.; Campbell, G. C., Jr.; Johnston, E.; Levorse, D.; McCauley, J.; Hussain, M. A spectroscopic investigation of losartan polymorphs. *Pharm. Res.* **1993,** *10*, (6), 900-4.

(35) Matsunaga, H.; Eguchi, T.; Nishijima, K.; Enomoto, T.; Sasaoki, K.; Nakamura, N. Solid-state characterization of candesartan cilexetil (TCV-116): Crystal structure and molecular mobility. *Chem. Pharm. Bull.* **1999,** *47*, 182-186.

(36) Bühlmayer, P.; Ostermayer, F.; Schmidlin, T. Acyl compounds. US5399578 A, 1995.

(37) Reguri, B.; Sunkari, S. Cardiovascular disorders; hypotensive agents. US20040072886 A1, 2004.

(38) Rukhman, I.; Flyaks, E.; Koltai, T.; Aronhime, J. Polymorphs of valsartan. US7105557 B2, 2006.

(39) Burgbacher, J.; Hahn, B. T.; Rampf, F. A.; Schneeberger, R. Highly crystalline valsartan. WO2012016969 A1 2012.

(40) United States Pharmacopeia and National Formulary (USP 32-NF 27). United States Pharmacopeial Convention: Rockville, 2009; 'Vol.' 2.

(41) Nogami, H.; Nagai, T.; Suzuki, A. Studies on Powdered Preparations. XVII. Dissolution Rate of Sulfonamides by Rotating Disk Method. *Chem. Pharm. Bull. (Tokyo)* **1966,** *14*, (4), 329-338.

(42) European Pharmacopoeia Commission, *European Pharmacopoeia*. 8th ed.; Council of Europe: Strasburg, 2013.

(43) Siepmann, J.; Siepmann, F. Mathematical modeling of drug dissolution. *Int. J. Pharm.* **2013,** *453*, (1), 12-24.

(44) Zhang, Y.; Huo, M.; Zhou, J.; Zou, A.; Li, W.; Yao, C.; Xie, S. DDSolver: An Add-In Program for Modeling and Comparison of Drug Dissolution Profiles. *The AAPS Journal* **2010,** *12*, (3), 263-271.

(45) Mildner, T.; Ernst, H.; Freude, D. ^{207}Pb NMR detection of spinning-induced temperature gradients in MAS rotors. *Solid State Nucl. Magn. Reson.* **1995,** *5*, (3), 269-71.

(46) Torchia, D. A. The measurement of proton-enhanced carbon-13 T_1 values by a method which suppresses artifacts. *J. Magn. Reson.* **1978,** *30*, (3), 613-616.

(47) Gervais, C.; Babonneau, F.; Maquet, J.; Bonhomme, C.; Massiot, D.; Framery, E.; Vaultier, M. ^{15}N cross-polarization using the inversion–recovery cross-polarization technique and ^{11}B magic angle spinning NMR studies of reference compounds containing B—N bonds. *Magn. Reson. Chem.* **1998,** *36*, (6), 407-414.

(48) Zorin, V. Gsim – a visualisation and processing program for solid-state NMR. http://gsim.sourceforge.net (2015.06.15).

(49) Pickard, C. J.; Mauri, F. All-electron magnetic response with pseudopotentials: NMR chemical shifts. *Phys. Rev. B* **2001,** *63*, (24), 245101.

(50) Harris, R. K.; Hodgkinson, P.; Pickard, C. J.; Yates, J. R.; Zorin, V. Chemical shift computations on a crystallographic basis: some reflections and comments. *Magn. Reson. Chem.* **2007,** *45*, S174-S186.

(51) Clark, S. J.; Segall, M. D.; Pickard, C. J.; Hasnip, P. J.; Probert, M. J.; Refson, K.; Payne, M. C. First principles methods using CASTEP. *Z. Kristallogr.* **2005,** *220*, (5-6), 567-570.

(52) Perdew, J. P.; Burke, K.; Ernzerhof, M. Generalized Gradient Approximation Made Simple. *Phys. Rev. Lett.* **1996,** *77*, (18), 3865-3868.

(53) Monkhorst, H. J.; Pack, J. D. Special points for Brillouin-zone integrations. *Phys. Rev. B* **1976,** *13*, (12), 5188-5192.

(54) Pyda, M.; Wunderlich, B. Reversing and Nonreversing Heat Capacity of Poly(lactic acid) in the Glass Transition Region by TMDSC. *Macromolecules* **2005,** *38*, (25), 10472-10479.

(55) Kawakami, K.; Pikal, M. J. Calorimetric investigation of the structural relaxation of amorphous materials: Evaluating validity of the methodologies. *J. Pharm. Sci.* **2005,** *94*, (5), 948-965.

(56) Hörter, D.; Dressman, J. B. Influence of physicochemical properties on dissolution of drugs in the gastrointestinal tract. *Adv. Drug Del. Rev.* **1997,** *25*, (1), 3-14.

(57) Potamitis, C.; Zervou, M.; Katsiaras, V.; Zoumpoulakis, P.; Durdagi, S.; Papadopoulos, M. G.; Hayes, J. M.; Grdadolnik, S. G.; Kyrikou, I.; Argyropoulos, D.; Vatougia, G.; Mavromoustakos, T. Antihypertensive drug valsartan in solution and at the AT_1 receptor: conformational analysis, dynamic NMR spectroscopy, in silico docking, and molecular dynamics simulations. *J. Chem. Inf. Model.* **2009,** *49*, (3), 726-39.

(58) Wang, S.-L.; Lin, S.-Y.; Chen, T.-F.; Chuang, C.-H. Solid-state trans–cis isomerization of captopril determined by thermal Fourier transform infrared (FT-IR) microspectroscopy. *J. Pharm. Sci.* **2001,** *90*, (8), 1034-1039.

(59) Brittain, H. G.; Morris, K. R.; Bugay, D. E.; Thakur, A. B.; Serajuddin, A. T. M. Solid-state NMR and IR for the analysis of pharmaceutical solids: Polymorphs of fosinopril sodium. *J. Pharm. Biomed. Anal.* **1993,** *11*, (11–12), 1063-1069.

(60) De Vita, E.; Frydman, L. Spectral Editing in ^{13}C MAS NMR under Moderately Fast Spinning Conditions. *J. Magn. Reson.* **2001,** *148*, (2), 327-337.

(61) Aso, Y.; Yoshioka, S.; Kojima, S. Relationship between the crystallization rates of amorphous nifedipine, phenobarbital, and flopropione, and their molecular mobility as measured by their enthalpy relaxation and ^1H NMR relaxation times. *J. Pharm. Sci.* **2000,** *89*, (3), 408-16.

(62) Hancock, B. C.; Shamblin, S. L. Molecular mobility of amorphous pharmaceuticals determined using differential scanning calorimetry. *Thermochim. Acta* **2001,** *380*, (2), 95-107.